Co-published by
Institute of Fluid-Flow Machinery
Polish Academy of Sciences
Committee on Thermodynamics and Combustion
Polish Academy of Sciences

http://www.imp.gda.pl/archives-of-thermodynamics/

Numerical analysis of the Soret and Dufour effects on boundary layer flow past a curved stretching surface in porous media with thermal slip and variable magnetic field

Temjennaro Jamir[a*], Hemanta Konwar[b], Bendangwapang Tzudir[b]

[a]Phek Government College, Phek, Phek 797108, India
[b]Kohima Science College, Jotsoma, Kohima 797001, India
*Corresponding author email: temjennaro@kscj.ac.in

Received: 28.09.2024; revised: 21.05.2025; accepted: 27.05.2025

Abstract

This study presents a novel investigation into the boundary layer flow, heat, and mass transfer of a Newtonian, incompressible and electrically conducting viscous fluid flow past a permeable curved stretching surface embedded in porous media with Soret and Dufour effects subject to varying magnetic fields and thermal slip. The research uniquely combines these complex phenomena, addressing a significant gap in the literature. This configuration has potential applications in electronic cooling systems, polymer manufacturing and compact heat exchangers in various industries. The main objectives are to understand how various parameters influence fluid flow, heat and mass transfer behaviour to optimize the design for enhanced performance. To attain the numerical results the governing equations are transformed into to a set of nonlinear ordinary differential equations, which are then solved numerically by using MATLAB's built-in solver bvp4c. The parameters of engineering interest are tabulated and validated with previous results. The outcomes of the study suggest that the presence of a larger magnetic parameter, Dufour number, Joule parameter, thermal slip and curvature parameter contribute to reducing the cooling rate of the system by 2.73%, 10.53%, 12.39%, 9.29% and 6.28%, respectively. Also, the curvature of the surface can be enlarged from 5 to 10 to obtain 6.87% reduction in surface drag force.

Keywords: Curved stretching surface; Variable magnetic field; Soret; Dufour; Porous media

Vol. 46(2025), No. 3, 77–87; doi: 10.24425/ather.2025.156580

Cite this manuscript as: Jamir, T., Konwar, H., & Tzudir, B. (2025). Numerical analysis of the Soret and Dufour effects on boundary layer flow past a curved stretching surface in porous media with thermal slip and variable magnetic field. *Archives of Thermodynamics*, 46(3), 77–87.

1. Introduction

In boundary layer flow, heat and mass transfer across a curved stretching surface is an important topic among researchers due to its numerous applications in polymer production, metallurgy and chemical engineering. Designing and creating new machinery and equipment with a high rate of heating or cooling draws the curiosity of many engineers and scientists. In industries, the intended final products are mostly determined by the rate of cooling. Additionally, a magnetic field has the potential to change heat transfer properties by rearranging fluid concentration. Furthermore, the direction and intensity of the applied magnetic field can be used to alter the fluid's behaviour. In industry, pure crystal semiconductor growth may be regulated by varying the magnetic field. Variable magnetic fields have been used to cure peptic ulcers, as well as for medical diagnostic and therapeutic purposes. Thus, studying the interactions between flow, heat, and mass transfer across curved stretching surfaces provides insights into complex physical phenomena and facilitates the development of innovative technologies and solutions across a wide range of industries.

Sajid et al. [1] were the first to explore the viscous flow caused by a curved stretching surface, discovering that dimensionless curvature increases boundary layer thickness while decreasing skin friction coefficients. Abbas et al. [2] investigated viscous fluid flow

Nomenclature

a – stretching rate
B – strength of magnetic field, T
B_0 – constant magnetic field, T
C – species concentration, kg m^{-3}
c_p – specific heat at constant pressure, J kg^{-1} K^{-1}
C_{fs} – local skin friction coefficient
C_∞ – ambient fluid concentration, kg m^{-3}
C_w – surface concentration, kg m^{-3}
c_s – concentration susceptibility
Da – Darcy parameter, $= \frac{\nu}{k_p a}$
D_m – mass diffusion coefficient, m^2 s^{-1}
Du – Dufour number, $= \frac{D_m k_T (C_w - C_\infty)}{c_s c_p \nu (T_w - T_\infty)}$
Ec – Eckert number, $= \frac{u_w^2}{c_p (T_w - T_\infty)}$
f – dimensionless stream function
J – Joule heating parameter, $= M^2$PrEc
K – curvature parameter, $= R\sqrt{\frac{a}{\nu}}$
k – thermal conductivity, W m^{-1} K^{-1}
k_p – coefficient of permeability
k_T – ratio of thermal diffusion
L – thermal slip parameter, $= L_1\sqrt{\frac{a}{\nu}}$
L_1 – thermal slip constant
M – magnetic parameter, $\sqrt{\frac{\sigma B_0^2}{\rho a}}$
Nu$_s$ – local Nusselt number
P – dimensionless pressure
p – pressure, N m^{-2}
Pr – Prandtl number, $= \frac{\mu c_p}{k}$
R – radius of curved surface, m
Re$_s$ – local Reynolds number, $= \frac{u_w s}{\nu}$
r, s – curvilinear coordinates
Sc – Schmidt number, $= \frac{\nu}{D_m}$
Sh$_s$ – local Sherwood number
Sr – Soret number, $= \frac{D_m k_T (T_w - T_\infty)}{T_m \nu (C_w - C_\infty)}$
T – fluid temperature, K
T_∞ – ambient fluid temperature, K
T_w – surface temperature, K
T_m – mean fluid temperature, K
u, v – velocity components in *r*- and *s*- directions, m s^{-1}
$(\cdot)', (\cdot)'', (\cdot)'''$ – differentiation with respect to variable η

Greek symbols

ν – kinematic viscosity of the fluid, m^2 s^{-1}
η – similarity variable
μ – dynamic viscosity
σ – electrical conductivity of the fluid, S m^{-1}
ρ – fluid density, kg m^{-3}
θ – dimensionless fluid temperature
ϕ – dimensionless fluid concentration
λ – suction/injection parameter

and heat transfer in the presence of a constant applied magnetic field over a curved stretched surface. Rosca and Pop [3] used mass suction to study the problem of unstable viscous flow across a curved stretching or shrinking surface and found that, in the case of a curved stretching surface, the pressure inside the boundary layer cannot be disregarded. Sanni et al. [4,5] studied the transfer of heat from a non-linear curved stretched surface in the absence and presence of a varying magnetic field. Hayat et al. [6] investigated the flow of viscous fluid across a nonlinear curved stretching surface under convective heat and mass circumstances. Saranya et al. [7] analysed bio-convective nanofluid flow over a curved surface employing the shifted Legendre collocation method, concluding that the concentration of motile bacteria significantly decreases with an increase in the curvature parameter. Abbas and Shatanawi [8] employed the bvp4c numerical technique to examine micropolar fluid on a curved surface. Majeed et al. [9] observed that the presence of a magnetic field reduces the heat transfer rate and shear stress in the analysis of bio-convective nanoparticle fluid flow across a stretched surface. Abbas et al. [10] examined cilia flow in a curved channel subjected to a radial magnetic field, revealing a substantial influence on the thermal characteristics of the system. Mahesha et al. [11] investigated nanofluid behaviour within an annular space formed by two concentric cylinders, indicating that quadratic resistance significantly affects both flow dynamics and heat transfer characteristics.

A medium with holes or blank spaces is said to be porous. Some examples of materials with pores include sand, wood, boulders, and soil. Porosity and permeability are two of a porous material's most crucial characteristics. Porosity is the quality of being porous, whereas permeability measures how easily gases, liquids, or certain compounds may transport through a material. Understanding porous media may help explain a lot of elements of transport processes. The porous material can regulate the heating or cooling process. Because of their importance in geophysics, petroleum technology, cooling of nuclear reactors, biochemical processes and other fields, transport mechanisms in porous media have received a lot of attention in recent years. Ahmed et al. [12] discussed boundary layer flow over a curved surface embedded in a porous medium and it was observed that increasing values of the porosity parameter decreases the fluid velocity. Using the homotopy analysis method, Riaz et al. [13] examined the motion of nanoparticles in a non-Darcy porous curved channel. Adeyemo et al. [14] emphasized understanding the impact of changing viscosity on nonlinear convective fluid flow in a porous medium. Sonam and Yadav [15] examined steady, laminar Casson fluid flow generated by a semi-infinite vertical plate, incorporating the effects of the Darcy-Forchheimer model and employing the bvp4c numerical method. Similarly, Jagadha et al. [16] developed a model for the steady flow of Jeffrey nanofluid over a nonlinearly stretching flat sheet of variable thickness, also governed by the Darcy-Forchheimer relation, using the Runge-Kutta numerical approach.

Due to its numerous applications, including the solidification of binary alloys, oil reservoirs, isotope separation, chemical reactors, and mixtures of gases, Soret and Dufour effects are significant fields of study in heat and mass transfer processes. Energy flux due to concentration gradient and mass flux due to temperature gradient in a medium are known as the Dufour and Soret effects, respectively. They are important mechanisms in transport phenomena and are often ignored because of their low order of magnitude. Imtiaz et al. [17] identified the impacts of Soret and Dufour in the flow of viscous fluid by a curved stretching surface. Magnetohydrodynamic (MHD) boundary layer mixed convection flow past an exponentially extending permeable sheet in porous media was presented by Konwar et al. [18] together with the Soret and Dufour effects. In another numerical investigation conducted by Jamir et al. [19], the significance of Soret and Dufour effects on the fluid flow system about a stretching sheet was presented. Soret and Dufour effects were found to impact the concentration and temperature profile for a system involving ferromagnetic hybrid nanofluid flow over a permeable surface [20].

In engineering and industries, the study of viscous dissipation is a crucial factor in understanding the energy balance within a system. The dissipation of mechanical energy into heat through viscous effects can have implications for the efficiency and heat generation in various processes, such as fluid transport in pipelines, blood flow in arteries, or any situation involving the flow of viscous fluids. Heat and mass transfer through a porous medium was discussed by Haile and Shankar [21] on MHD flow of nanofluids with the effects of viscous dissipation, thermal radiation and chemical reaction. A study conducted by Oladapo et al. [22], who reported that the presence of slip effect significantly influences the flow and heat transfer of the system, referred to the case of a non-Newtonian fluid for enhanced heat transfer devices. Sademaki [23] elucidated the impact of viscous dissipation on sustained heat transfer in chemically reactive MHD nanofluid flow, incorporating mass and heat diffusion characteristics within a vertical cone filled with a saturated porous medium. Another study indicated that the Soret and Dufour effects impact the heat transfer rate in the flow of viscoelastic fluid caused by a stretching surface with viscous dissipation [24].

In the above literature survey, it is evident that MHD flow over curved surfaces is of great interest to researchers and is applicable in various fields of engineering. Taking into account the significance of the flow on curved surface, the present problem aims to provide insight into the problem of boundary layer flow, heat, and mass transfer over a permeable curved stretching sheet in porous media with Soret and Dufour effects subject to variable magnetic fields and thermal slip, which has not been accounted for in any of the literature cited above. The study aims to analyse the outcomes as well as find answers to how these parameters may possibly contribute to improving or reducing the boundary layers of the system under consideration. The study also looks into the parameters of engineering interest, which will significantly contribute towards finding new innovations to enhance cooling rates in curved devices and equipment, such as cooling electronics, heat exchanger design, polymer manufacturing and metal forming.

2. Mathematical formulation

This issue pertains to examining the flow of a two-dimensional, steady, Newtonian, incompressible, and electrically conducting viscous fluid flow past a permeable curved stretching sheet curled

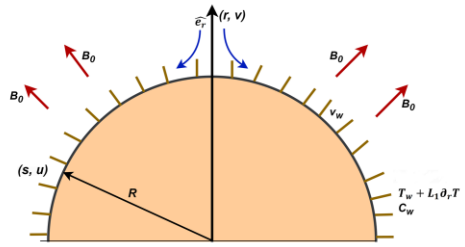

Fig. 1. Geometric configuration of the flow.

in a circle of radius R and the sheet is being stretched in s-direction with a velocity $u = as$, where $a > 0$ (see Fig. 1). Also, a variable magnetic field of strength $B(r) = RB_0(R + r)^{-1}\hat{e_r}$ is applied in the radial direction of the curved sheet and takes a constant value, when $R \to \infty$, where $\hat{e_r}$ is the unit vector in the radial direction. Assuming the magnetic Reynolds number is negligible, the influence of the induced magnetic field can be disregarded. Additionally, the work presents thermal slip conditions at the surface-fluid interface. This enhancement enriches our analysis and enables a more detailed examination of fluid flow.

The present analysis includes a thorough array of assumptions, such as:

1. Integration of porous media effects, recognizing the impact of permeability on flow dynamics.
2. Assessment of suction-injection effects, essential for evaluating fluid transport phenomena.
3. Incorporation of viscous dissipation, Soret and Dufour effects to improve heat and mass transfer, particularly relevant to energy systems, augmentation of heat transfer, polymer processing, and advanced thermal management technologies.
4. Utilization of boundary layer approximation methods to analyse fluid flow near walls.
5. Consideration of thermal slip effect to reflect the realistic scenarios.

The flow in curvilinear coordinates is modelled by the governing equations, which are expressed as [5,7]:

$$\partial_r[(R + r)v] + R\partial_s u = 0, \tag{1}$$

$$\frac{u^2}{R+r} = \frac{1}{\rho}\partial_r p, \tag{2}$$

$$v\partial_r u + \left(\frac{Ru}{R+r}\right)\partial_s u + \frac{uv}{R+r} = -\frac{1}{\rho}\left(\frac{R}{R+r}\right)\partial_s p + \nu\left[\partial_r^2 u + \left(\frac{1}{R+r}\right)\partial_r u - \frac{u}{(R+r)^2}\right] - \frac{\sigma B_0^2 R^2 u}{\rho(R+r)^2} - \frac{\nu u}{k_p}, \tag{3}$$

$$\left[v\partial_r T + \left(\frac{Ru}{R+r}\right)\partial_s T\right] = \frac{k}{\rho c_p}\left[\partial_r^2 T + \left(\frac{1}{R+r}\right)\partial_r T\right] + \\ + \frac{\mu}{\rho c_p}\left(\partial_r u - \frac{u}{R+r}\right)^2 + \frac{D_m k_T}{c_s c_p}\left[\partial_r^2 C + \left(\frac{1}{R+r}\right)\partial_r C\right] + \frac{\sigma B_0^2 R^2 u^2}{\rho c_p (R+r)^2}, \quad (4)$$

$$v\partial_r C + \left(\frac{Ru}{R+r}\right)\partial_s C = D_m\left(\partial_r^2 C + \frac{1}{R+r}\partial_r C\right) + \\ + \frac{D_m k_T}{T_m}\left(\partial_r^2 T + \frac{1}{R+r}\partial_r T\right). \quad (5)$$

The appropriate boundary conditions are [8]:

$$u = u_w = as,\ v = -v_w,\ T = T_w + L_1\partial_r T,\ C = C_w \\ \text{at } r = 0, \quad (6)$$

$$u \to 0,\ \partial_r u \to 0,\ T \to T_\infty,\ C \to C_\infty \text{ as } r \to \infty, \quad (7)$$

where $v_w = \frac{Rv_0}{R+r}$ and v_0 is the initial value and variable velocity at the wall, respectively.

The following similarity transformations [1]:

$$u = asf'(\eta),\ v = \frac{-R}{R+r}\sqrt{a\nu}\,f(\eta),\ \eta = \sqrt{a/\nu}\,r, \\ p = \rho a^2 s^2 P(\eta),\ \theta(\eta) = \frac{T-T_\infty}{T_w-T_\infty},\ \phi(\eta) = \frac{C-C_\infty}{C_w-C_\infty} \quad (8)$$

satisfy Eq. (1), and Eqs. (2) and Eq. (3) transform to:

$$P' = \frac{f'^2}{\eta+K}, \quad (9)$$

$$\frac{2K}{\eta+K}P = f''' + \frac{f''}{\eta+K} - \frac{f'}{(\eta+K)^2} - \frac{Kf'^2}{\eta+K} + \frac{Kff''}{\eta+K} + \\ + \frac{Kff'}{(\eta+K)^2} - \frac{M^2K^2f'}{(\eta+K)^2} - \mathrm{Da}f'. \quad (10)$$

Eliminating pressure P from Eqs. (9) and (10), the following dimensionless momentum equation is obtained:

$$f'^v + \frac{2f'''+K(ff'''-f'f'')}{\eta+K} - \frac{f''-K\left(ff''-f'^2\right)}{(\eta+K)^2} + \frac{f'-Kff'}{(\eta+K)^3} + \\ - \frac{M^2K^2}{(\eta+K)^2}\left[f'' - \frac{f'}{(\eta+K)}\right] - \mathrm{Da}\left(f'' + \frac{f'}{\eta+K}\right) = 0. \quad (11)$$

Prime in this case represents derivatives with regard to the similarity variable η.

With the transformations (8), the energy and species concentration equations in dimensionless form become:

$$\theta'' + \frac{\theta'}{\eta+K} + \frac{\mathrm{Pr}K f\theta'}{\eta+K} + \mathrm{PrEc}\left(f'' - \frac{f'}{\eta+K}\right)^2 + \\ + \mathrm{PrDu}\left(\phi'' + \frac{\phi'}{\eta+K}\right) + \frac{JK^2f'^2}{(\eta+K)^2} = 0, \quad (12)$$

$$\phi'' + \frac{\phi'}{\eta+K} + \frac{\mathrm{Sc}K f\phi'}{\eta+K} + \mathrm{ScSr}\left(\theta'' + \frac{\theta'}{\eta+K}\right) = 0 \quad (13)$$

together with transformed boundary conditions:

$$f(\eta) = \lambda,\ f'(\eta) = 1,\ \theta(\eta) = 1 + L\theta'(\eta),\ \phi(\eta) = 1 \text{ at } \eta = 0, \quad (14)$$

$$f'(\eta) \to 0,\ f''(\eta) \to 0, \theta(\eta) \to 0, \text{ as } \eta \to \infty, \quad (15)$$

were suction is represented by $\lambda = \frac{v_0}{\sqrt{a\nu}} > 0$ and injection by $\lambda < 0$ [18].

The skin friction coefficient $C_{fs} = \tau_{rs}/(\rho u_w^2)$, Nusselt number $\mathrm{Nu}_s = sq_w/\{k(T_w - T_\infty)\}$, and Sherwood number $\mathrm{Sh}_s = sq_m/\{D_m(C_w - C_\infty)\}$ are engineering characteristics that contribute significantly to understanding heat and mass transfer. Here, $\tau_{rs} = \mu\left(\partial_r u - \frac{u}{r+R}\right)_{r=0}$ is the wall shear stress, $q_w = -k(\partial_r T)_{r=0}$ is the wall heat flux and $q_m = -D_m(\partial_r C)_{r=0}$ represents the wall mass flux.

Upon using Eqs. (8), the following are determined:

– the skin friction coefficient:

$$\mathrm{Re}_s^{\frac{1}{2}} C_{fs} = f''(0) - \frac{f'(0)}{K}, \quad (16)$$

– the Nusselt number:

$$\mathrm{Re}_s^{-\frac{1}{2}}\mathrm{Nu}_s = -\theta'(0), \quad (17)$$

and the Sherwood number:

$$\mathrm{Re}_s^{-\frac{1}{2}}\mathrm{Sh}_s = -\phi'(0). \quad (18)$$

3. Numerical procedure

The bvp4c method (a finite difference method that provides C^1-continuous solution) [25] is utilized to derive the computational solution of Eqs. (11)–(13), subject to the limitations defined by Eqs. (14) and (15). Current flow difficulties include dimensionless ordinary differential equations that exhibit a particularly high nonlinear nature. The principal research objective is to precisely tackle challenges pertaining to non-linear flow phenomena. The bvp4c numerical approach within the MATLAB software is the most suitable for acquiring the quantitative solution of the present model [25]. It is important to supply three distinct categories of data: the first-order equations to be solved, the corresponding boundary conditions, and the first guess employed to ascertain the solution to the problem. The integration interval is defined from zero to five and from zero to ten, with a relative tolerance set at 10^{-7}. The mesh is automatically changed to enhance accuracy based on this tolerance.

We reformulate the provided equations for the bvp4c code as a system of first-order ordinary differential equations (ODEs):

$$f = y_1,\ f' = y_2,\ f'' = y_3,\ f''' = y_4, \\ \theta = y_5,\ \theta' = y_6,\ \phi = y_7,\ \phi' = y_8. \quad (19)$$

By substituting Eqs. (19) into equations Eqs. (11)–(13), the resultant system of 1st-order ODE can be derived:

$$y_1' = y_2, \quad (20)$$

$$y_2' = y_3, \quad (21)$$

$$y_3' = y_4, \quad (22)$$

$$y_4' = -\frac{2y_4+K(y_1y_4-y_2y_3)}{\eta+K} + \frac{y_3-K(y_1y_3-y_2^2)}{(\eta+K)^2} - \frac{y_2-Ky_1y_2}{(\eta+K)^3} + \\ + \frac{M^2K^2}{(\eta+K)^2}\left(y_3 - \frac{y_2}{\eta+K}\right) + \mathrm{Da}\left(y_3 + \frac{y_2}{\eta+K}\right), \quad (23)$$

$$y_5' = y_6, \quad (24)$$

$$y_6' = \frac{1}{1-\mathrm{PrDuSrSc}}\left[-\frac{y_6}{\eta+K} - \frac{\mathrm{Pr}Ky_1y_6}{(\eta+K)} - \mathrm{PrEc}\left(y_3 - \frac{y_2}{(\eta+K)}\right)^2 + -\frac{JK^2{y_2}^2}{(\eta+K)^2} - \mathrm{PrDu}\left(-\frac{KScy_1y_8}{\eta+K} - \frac{\mathrm{ScSr}y_6}{\eta+K}\right)\right], \quad (25)$$

$$y_7' = y_8, \quad (26)$$

$$y_8' = -\frac{y_8}{\eta+K} - \frac{KScy_1y_8}{\eta+K} - \mathrm{ScSr}\left\{\frac{1}{(1-\mathrm{PrDuSrSc})}\left[-\frac{y_6}{\eta+K} + -\frac{\mathrm{Pr}Ky_1y_6}{\eta+K} - \mathrm{PrEc}\left(y_3 - \frac{y_2}{\eta+K}\right)^2 - \frac{JK^2{y_2}^2}{(\eta+K)^2} + -\mathrm{PrDu}\left(-\frac{KScy_1y_8}{\eta+K} - \frac{\mathrm{ScSr}y_6}{\eta+K}\right)\right] + \frac{y_6}{\eta+K}\right\} \quad (27)$$

with the transformed boundary conditions as follows:

$$y_1(0) - \lambda,\ y_2(0) - 1,\ y_5(0) - 1 - Ly_6(0), y_7(0) - 1, \quad (28)$$

$$y_2(\infty);\ y_3(\infty); y_5(\infty); y_7(\infty). \quad (29)$$

4. Validation of results

To validate the methodology used in this study, numerical values that have been obtained in the study have been compared to those obtained by Abbas et al. [2] and Sanni et al. [5], using the shooting method with the Runge-Kutta algorithm in MATLAB. This is shown in Table 1, which tabulates the values of the surface drag force and the heat transfer rate upon varying the curvature parameter and the magnetic parameter. The data recorded in Table 1 are seen to be in good convergence, which shows the accuracy of the present numerical scheme.

Table 1. Comparison of $-\mathrm{Re}_s^{\frac{1}{2}}C_{fs}$ and $\mathrm{Re}_s^{-\frac{1}{2}}\mathrm{Nu}_s$ for different values of K and M, when Pr = 0.7, Ec = 0.2, in absence of other parameters.

		Abbas et al. [2]		Sanni et al. [5]		Present result	
K	M	$-\mathrm{Re}_s^{\frac{1}{2}}C_{fs}$	$\mathrm{Re}_s^{-\frac{1}{2}}\mathrm{Nu}_{fs}$	$-\mathrm{Re}_s^{\frac{1}{2}}C_{fs}$	$\mathrm{Re}_s^{-\frac{1}{2}}\mathrm{Nu}_{fs}$	$-\mathrm{Re}_s^{\frac{1}{2}}C_{fs}$	$\mathrm{Re}_s^{-\frac{1}{2}}\mathrm{Nu}_{fs}$
5	0.2	1.22881	0.43268	1.20372	0.42418	1.20442	0.42716
10	0.2	1.12311	0.41896	1.10709	0.41132	1.10485	0.41137
20	0.2	1.07541	0.41094	1.06389	0.40365	1.06045	0.40009
50	0.2	1.04849	0.40571	1.03958	0.39864	1.02779	0.39370
100	0.2	1.03982	0.40390	1.03175	0.39691	1.02389	0.39113
200	0.2	1.03553	0.40298	1.02788	0.39604	1.02080	0.38981
10	0.2	1.12311	0.41896	1.10709	0.41132	1.11909	0.41137
10	0.4	1.18306	0.40717	1.16408	0.39975	1.17579	0.39754
10	0.6	1.27633	0.38927	1.25344	0.38190	1.26228	0.38109
10	0.8	1.39562	0.36727	1.36870	0.35953	1.37096	0.35223

5. Results and discussion

This paper examines the steady, two-dimensional boundary layer flow, heat and mass transfer, thermal slip, and variable magnetic field of a Newtonian, incompressible, viscous, and electrically conducting fluid past a permeable curved stretching surface in porous media. The distributions of fluid temperature, concentration, and velocity are represented graphically with the numerical findings, and the behaviour of different parameters is examined. Different parameter values are taken into consideration, with Prandtl number Pr = 0.7 taken for air and Schmidt number Sc = 0.6 taken for water vapour, K = 5, Da = 0.5, M = 0.2, J = 0.2, Ec = 0.2, Sr = 0.4, Du = 0.2, λ = 0.2, L = 0.2, unless stated otherwise.

Figures 2−7 illustrate the outcome of the curvature parameter (K) and the magnetic parameter (M) on the boundary layers of the fluid. It has been observed that $f'(\eta)$, $\theta(\eta)$, and $\phi(\eta)$ exhibit an increase as K becomes greater. As K grows, the surface shape transforms, hence modifying the fluid flow over it. Enhanced curvature results in elevated gradients within the velocity field owing to the more significant bending of the surface. This improves velocity distributions. The extended surface will improve the thermal and species dispersion of the fluid due to its significant capacity for fluid movement and contact with the surface. Consequently, the thickness of the thermal and concentration boundary layers will increase.

A reverse effect is noticed for the magnetic parameter. The resistive force known as the Lorentz force, produced due to the effect of the magnetic field on an electrically conducting fluid, suppresses the bulk motion of the fluid and, as a result, both the components of fluid velocity decrease. Moreover, because of the friction caused by this resistive force, more heat is generated, which eventually increases the temperature and concentration distribution in the flow. According to tabulated data in Table 3, upon increasing curvature of the surface ($5 \le K \le 10$) and magnetic field intensity ($0.2 \le M \le 0.5$), both the heat transfer rate and mass transfer rate reduce, by 6.28% and 2.73%, and by 7.3% and 1.15%, respectively. Thus, one can increase the cooling rate in conducting fluid flows by considering lesser curvature parameter and magnetic field. Moreover, for a larger curved surface, the

Table 2. Numerical values of $-\mathrm{Re}_s^{\frac{1}{2}}C_{fs}$ with Pr = 0.7, Ec = 0.2, Du = 0.2, J = 0.2, Sc = 0.6, Sr = 0.4 and L = 0.2.

K	M	Da	λ	$-\mathrm{Re}_s^{\frac{1}{2}}C_{fs}$
5	0.2	0.5	0.2	1.54627
10	0.2	0.5	0.2	1.44009
5	0.5	0.5	0.2	1.61541
5	0.2	0.7	0.2	1.62783
5	0.2	0.5	0.4	1.63839

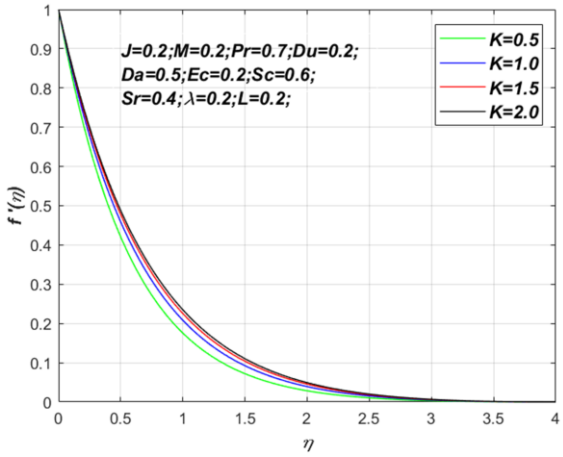

Fig. 2. Velocity distribution over varying *K*.

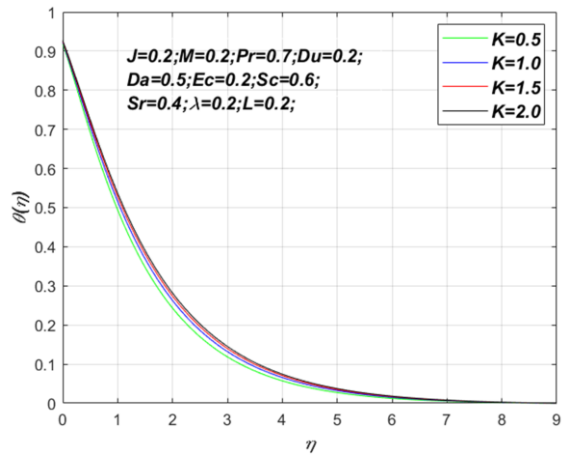

Fig. 3. Temperature distribution over varying *K*.

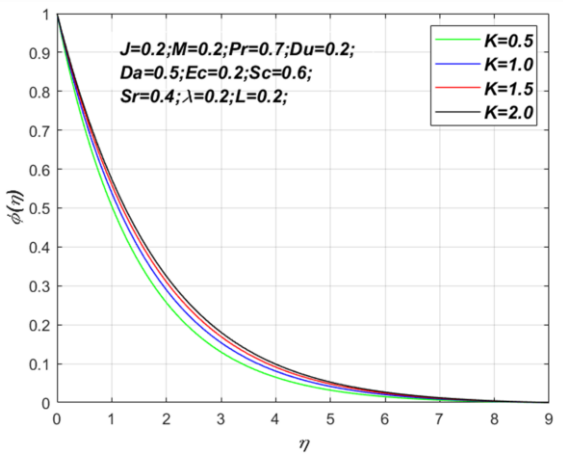

Fig. 4. Concentration distribution over varying *K*.

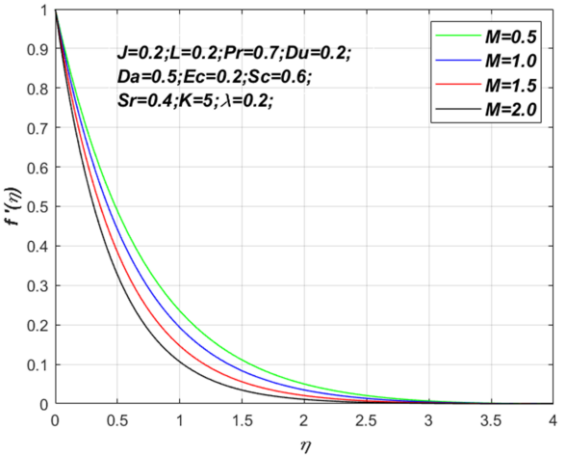

Fig. 5. Velocity distribution over varying *M*.

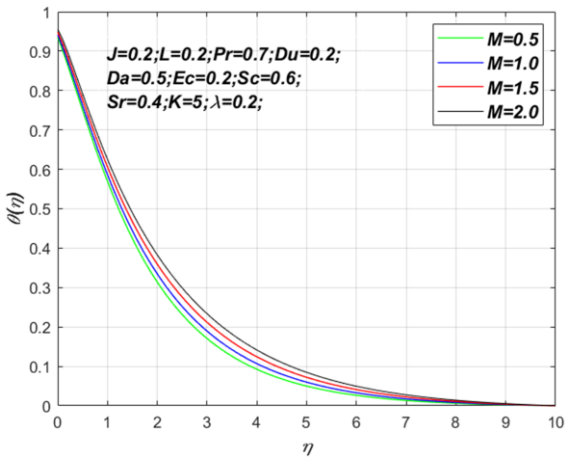

Fig. 6. Temperature distribution over varying *M*.

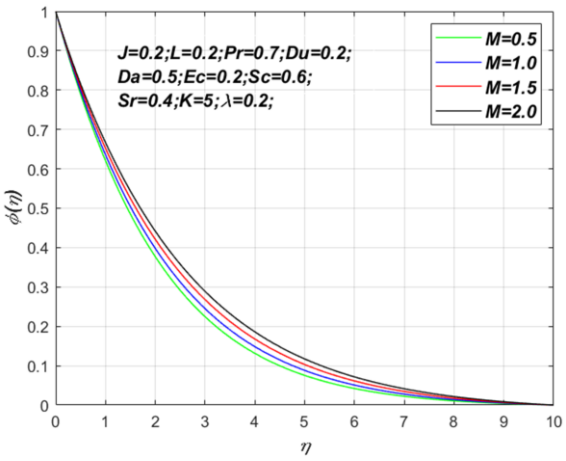

Fig. 7. Concentration distribution over varying *M*.

surface drag force decreases by about 6.87%, while as the magnetic field intensifies, the surface drag also improves by around 4.47% (see Table 2).

Figures 8−10 represent the effects of Darcy parameter (Da) on velocity component ($f'(\eta)$), temperature ($\theta(\eta)$) and concentration ($\phi(\eta)$) distributions. The porous medium physically exemplifies a type of external resistance that restricts fluid movement, resulting in a reduction of fluid velocity. It is established that an increase in Darcy number alters the permeability rate of the fluid through the porous medium, consequently diminishing the velocity distribution. However, the temperature of the fluid increases due to the rising values of Da. This is because increased porosity facilitates greater

Table 3. Numerical values of $\mathrm{Re}_s^{-\frac{1}{2}}\mathrm{Nu}_s$ and $\mathrm{Re}_s^{-\frac{1}{2}}\mathrm{Sh}_s$ when $\lambda = 0.2$.

K	M	Da	Pr	Ec	Du	J	Sc	Sr	L	$\mathrm{Re}_s^{-\frac{1}{2}}\mathrm{Nu}_{fs}$	$\mathrm{Re}_s^{-\frac{1}{2}}\mathrm{Sh}_{fs}$
5	0.2	0.5	0.7	0.2	0.2	0.2	0.6	0.4	0.2	0.33151	0.47911
10	0.2									0.31066	0.44414
5	0.5									0.32246	0.47359
	0.2	0.7								0.32085	0.47264
		0.5	1.38							0.46581	0.44967
			0.7	0.4						0.22965	0.50344
				0.2	0.4					0.29661	0.48721
					0.2	0.4				0.29044	0.48892
						0.2	0.94			0.31418	0.62965
							0.6	0.8		0.33513	0.44537
								0.4	0.4	0.30072	0.48362

fluid movement across the medium, hence enhancing convective heat transfer, which effectively transports heat and causes a temperature increase within the porous medium. Also, an increase in the concentration distribution is noted when the values of Da increase. This is due to the rate of permeability of the porous medium, which makes the thickness of the boundary layer continuously increasing (see Fig. 10). From Tables 2 and 3, it has

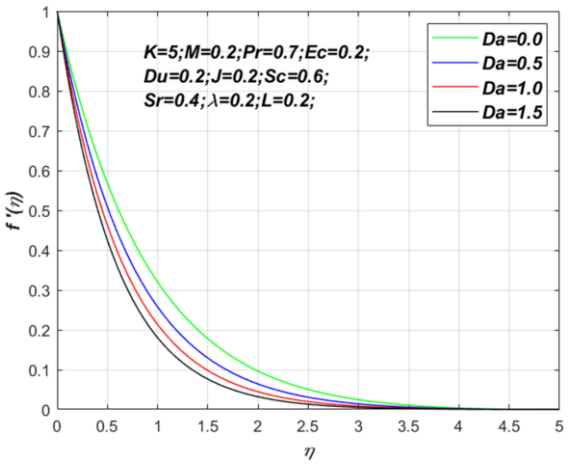

Fig. 8. Velocity distribution over varying Da.

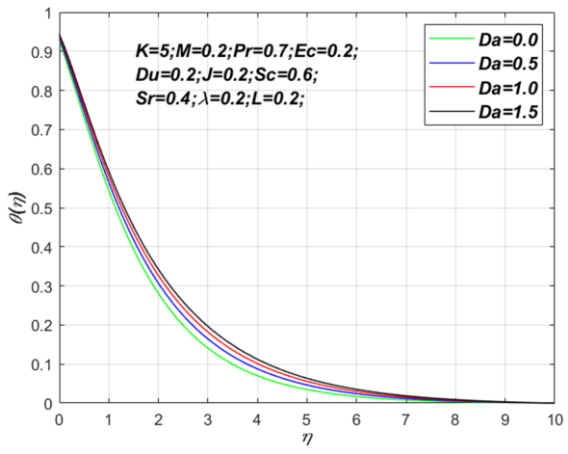

Fig. 9. Temperature distribution over varying Da.

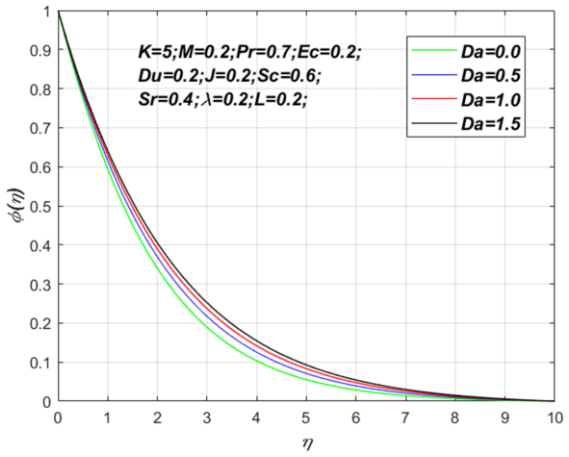

Fig. 10. Concentration distribution over varying Da.

been observed that surface drag increases by about 5.27%, while the heat and mass transfer rates both reduce by 3.22% and 1.35%, respectively, within $0.5 \leq \mathrm{Da} \leq 0.7$.

Figures 11 and 12 depict the impact of the Prandtl number (Pr) on the temperature distribution ($\theta(\eta)$) and the concentration distribution ($\phi(\eta)$), correspondingly. The parametric values evaluated for Pr are 0.015, 0.7, 1.38 and 7.0, which correspond

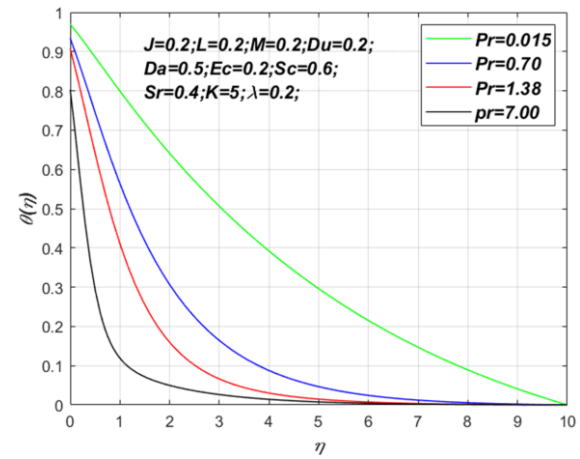

Fig. 11. Temperature distribution over varying Pr.

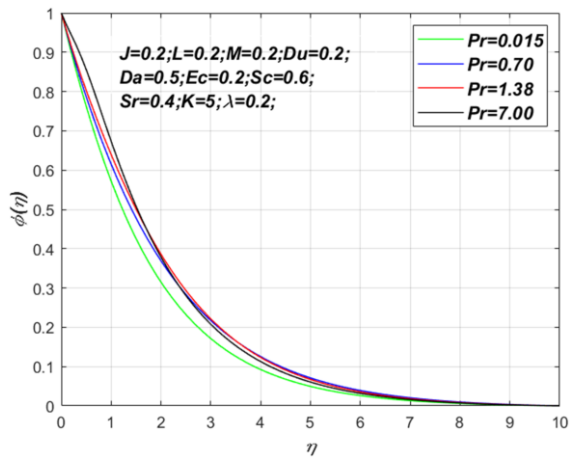

Fig. 12. Concentration distribution over varying Pr.

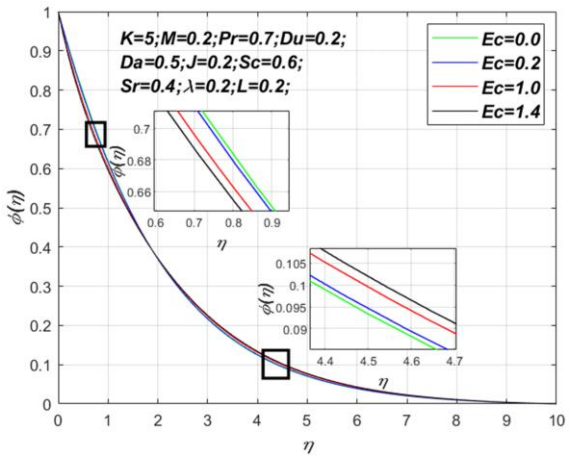

Fig. 14. Concentration distribution over varying Ec.

to liquid metal, air, ammonia, and water, respectively. The results indicate a significant decrease in temperature for large Prandtl numbers, resulting in the weakening of the thermal boundary layer. The concentration of fluid along the wall increases and falls away from the sheet when the value of η is greater than 2.3 for materials with high Pr values. Physically, a higher Pr value indicates a lower thermal diffusivity, which means that heat is dispersed more slowly from the surface, resulting in a drop in the temperature of the fluid. Table 3 demonstrates that when the values of Pr grow ($0.7 \leq \mathrm{Pr} \leq 1.38$), the heat transfer rate experiences a substantial increase of 40.51%; however, the mass transfer rate decreases by approximately 6.14%. Fluids with lower Prandtl numbers have stronger thermal conductivities, facilitating faster heat dissipation from the surface compared to fluids with higher Pr values. Prandtl number can therefore be used to increase the cooling rate in conducting fluid flows.

The outcome of the rising values of the Eckert number (Ec) on the temperature ($\theta(\eta)$) and concentration ($\phi(\eta)$) distributions is depicted in Figs. 13 and 14. It is known that temperature is considered the average of kinetic energy, while on the other hand, Ec exhibits a relation with kinetic energy. Thus, keeping these two conditions, it can be concluded that upon improving the energy dissipation, the kinetic energy increases, which in turn significantly improves the temperature distribution. It is also important to note that because of this factor, the concentration of the fluid near the vicinity of the surface declines, while upon entering the region $\eta > 1.9$, a reverse trend is noticed in the concentration distribution. Also, from Table 3, it can be concluded that Ec is an important parameter in the heat transport phenomenon and can be incorporated to significantly reduce, by 30.73%, the rate of cooling and enhance by 5.08% the mass transfer rate.

In Figs. 15 and 16, the influence of the Joule heating parameter (J) on the distributions of temperature and concentration is presented. Physically, as the Joule heating parameter enhances the impact of the energy dissipation, as well as the magnetic field, intensifies, thus the resulting Lorentz force aids in promoting the heating of the curved surface; also, due to inside friction of molecules, the mechanical energy, which gets converted to thermal energy aids in improving the temperature distribution significantly (mainly near the vicinity of the curved surface).

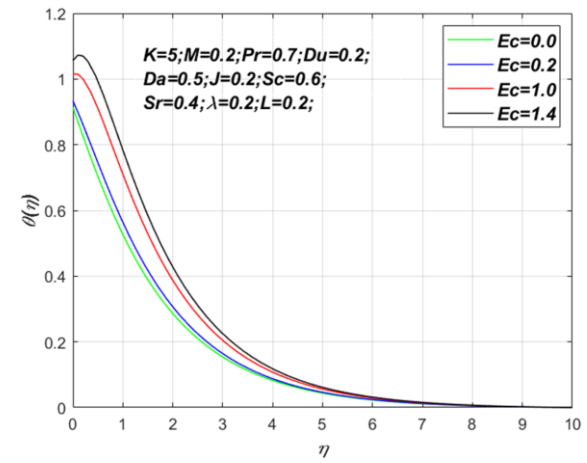

Fig. 13. Temperature distribution over varying Ec.

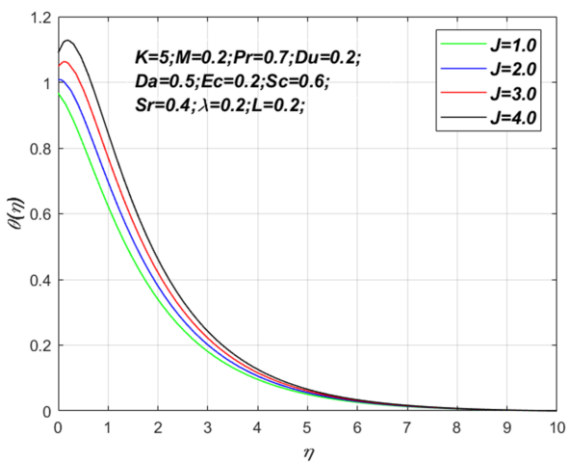

Fig. 15. Temperature distribution over varying J.

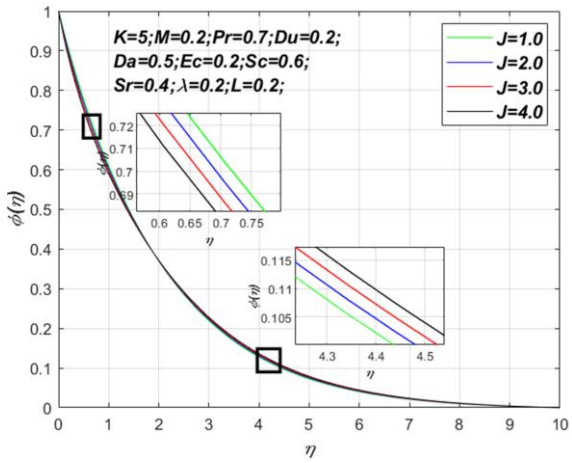

Fig. 16. Concentration distribution over varying *J*.

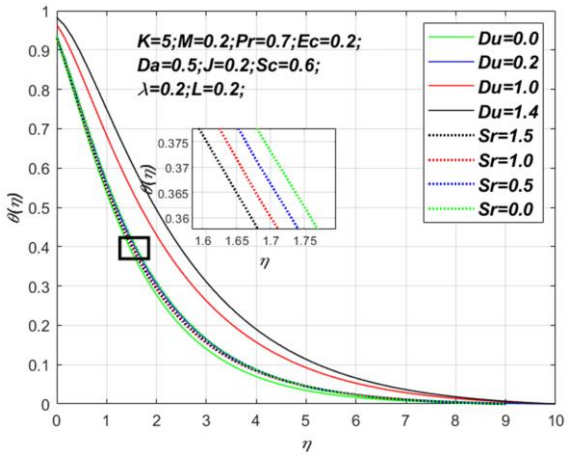

Fig. 18. Temperature distribution over varying Du and Sr.

Because of these factors, although the concentration distribution is found to be declining near the vicinity of the surface in a region beyond $\eta > 1.9$, the species concentration distribution slowly rises. From Table 3, it can be concluded that improving J can significantly reduce, by 12.39%, the cooling rate and enhance by 2.05% the mass transfer rate.

The effects of Schmidt number (Sc) on concentration ($\phi(\eta)$) distribution of the fluid are shown in Fig. 17. Parametric values considered for Sc are 2.35, 1.32, 0.94, and 0.22 corresponding to naphthalene, ethanol, hydrogen sulphide, and helium, respectively. Data plotted show that as the Sc concentration increases, the fluid concentration within the boundary layer drops. The reason for this is that a greater value of Sc indicates a higher kinematic viscosity, which hinders the movement of mass and, consequently, results in a reduction of the fluid concentration. A significant hike in the mass transfer rate (by 31.42%) is also recorded in Table 3 for $0.6 \leq Sc \leq 0.94$.

Figures 18 and 19 depict the effects of Dufour (Du) and Soret (Sr) on the temperature ($\theta(\eta)$) and species concentration ($\phi(\eta)$) distributions, respectively. It has been observed that an increase in the Dufour number causes a rise in the temperature of the

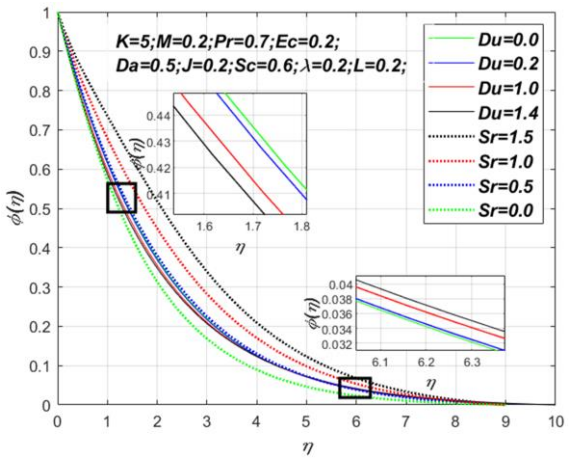

Fig. 19. Concentration distribution over varying Du and Sr.

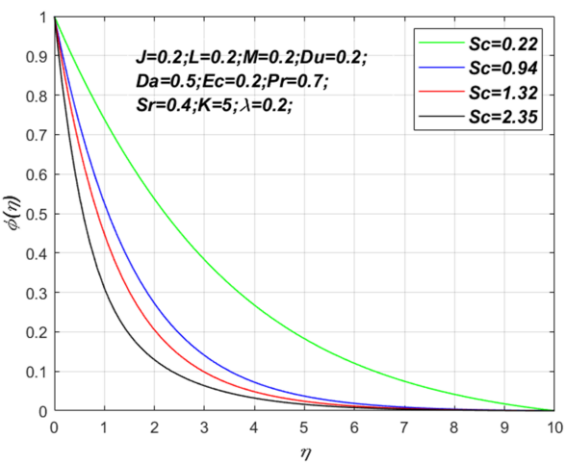

Fig. 17. Concentration distribution over varying Sc.

fluid, while under the same influence, a varying outcome is observed on the concentration distribution. As reflected in Fig. 19, the concentration of species declines near the vicinity of the curved surface; however, beyond $\eta > 4.5$, the species concentration begins to rise. When the Dufour number is relatively elevated, thermal diffusion prevails over mass diffusion. This may lead to fluctuations in temperature gradients, which can subsequently generate buoyancy effects, altering the density distribution and perhaps affecting flow patterns through natural convection. The Dufour phenomenon results in a broader temperature distribution compared to its absence. From Figs. 18 and 19, it is also clear that Sr significantly improves species concentration, while reducing the temperature profile to a certain extent. The distribution of concentrations in the Soret phenomenon is influenced by the temperature gradient. In fact, higher Soret numbers cause more convective flow since they are linked to larger temperature gradients. The dispersion of the concentration rises as a result. Analysis from Table 3 shows that a higher $0.2 \leq Du \leq 0.4$ aids in reducing the heat transfer rate significantly (by 10.53%), while enhancing the mass transfer rate (by 1.69%). On the contrary, higher $0.4 \leq Sr \leq 0.8$ aids in enhancing the heat

transfer rate (by 1.09%) and significantly reduces the mass transfer rate (by 7.04%).

Figure 20 depicts the graphical data of the temperature ($\theta(\eta)$) distribution upon enhancing the thermal slip parameter (L). It is clear from Fig. 20 that increasing L results in a substantial decrease in the temperature distribution in the region closer to the curved wall. Physically, this decrease in surface temperature happens as a result of thermal slip, which facilitates heat transfer from the fluid surface to its interior. The temperature inside the thermal boundary layer drops as a result of the improved heat transfer brought on by thermal slip. The data presented in Table 3 indicates a notable decrease of around 9.29% in heat transfer rates for $0.2 \leq L \leq 0.4$.

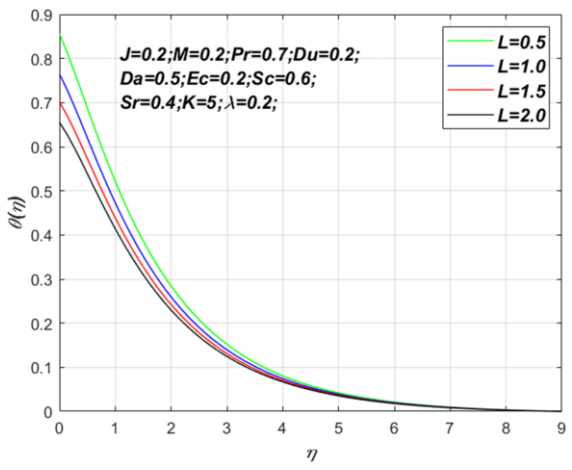

Fig. 20. Temperature distribution over varying L.

6. Conclusions

Based on the preceding discussions, the following conclusions can be drawn:

- Velocity of fluid increases for higher curvature parameter and decreases with increasing Darcy parameter and magnetic parameter.
- The curvature parameter, magnetic parameter and Darcy parameter can be increased for the reduction of the heat transfer rate (by around 6.28%, 2.73%, and 3.22%, respectively), as well as the mass transfer rates (by around 7.30%, 1.15%, and 1.35%, respectively).
- For large Prandtl numbers, there is a significant decrease in temperature. Therefore, the Prandtl number can be utilized to enhance the cooling rate (by around 40.51%) in the flow of conducting fluids.
- The Eckert number, Dufour number and the Joule heating parameter tend to reduce the species concentration in the vicinity of the curved region, while at a distance away from the surface, they also aid in gradually boosting the species concentration.
- The Soret number increases the concentration of the fluid. The heat transfer rate increases (by 1.09%), but the mass transfer rate decreases (by 7.04%) for larger values of the Soret number.
- The Dufour number significantly contributes towards raising the temperature of the fluid and aids in reducing the cooling rate by 10.53%.
- The mass transfer rate increases for higher values of the Dufour number (by 1.69%), the Schmidt number (by 31.42%), the Joule heating parameter (by 2.05%) and the Eckert number (by 5.08%).

The physics of flow on curved surfaces with variable magnetic field and heat slip can be employed in various physical domains, including industries, aeronautics, medicinal research, and engineering sciences.

Acknowledgements

The authors are grateful to the authority of the Directorate of Higher Education, Nagaland and Kohima Science College, Jotsoma, Nagaland for financial support to pursue this work.

References

[1] Sajid, M., Ali, N., Javed, T., & Abbas, Z. (2010). Stretching a curved surface in a viscous fluid. *Chinese Physics Letters*, 27(2), 024703. doi: 10.1088/0256-307X/27/2/024703

[2] Abbas, Z., Naveed, M., & Sajid, M. (2013). Heat transfer analysis for stretching flow over a curved surface with magnetic field. *Journal of Engineering Thermophysics*, 22(4), 337–345. doi: 10.1134/S1810232813040061

[3] Roşca, N.C., & Pop, I. (2015). Unsteady boundary layer flow over a permeable curved stretching/shrinking surface. *European Journal of Mechanics, B/Fluids*, 5161–67. doi: 10.1016/j.euromechflu.2015.01.001

[4] Sanni, K.M., Asghar, S., Jalil, M., & Okechi, N.F. (2017). Flow of viscous fluid along a nonlinearly stretching curved surface. *Results in Physics*, 7(12), 1–4. doi: 10.1016/ j.rinp.2016.11.058

[5] Sanni, K.M., Hussain, Q., & Asghar, S. (2020). Heat transfer analysis for non-linear boundary driven flow over a curved stretching sheet with a variable magnetic field. *Frontiers in Physics*, 8, 00113. doi: 10.3389/fphy.2020.00113

[6] Hayat, T., Saif, R.S., Ellahi, R., Muhammad, T., & Ahmad, B. (2017). Numerical study of boundary-layer flow due to a nonlinear curved stretching sheet with convective heat and mass conditions. *Results in Physics*, 7, 2601–2606. doi: 10.1016/j.rinp.2017.07.023

[7] Saranya, S., Ragupathi, P., & Al-Mdallal, Q. (2022). Analysis of bioconvective heat transfer over an unsteady curved stretching sheet using the shifted Legendre collocation method. *Case Studies in Thermal Engineering*, 39, 102433. doi: 10.1016/j.csite.2022.102433

[8] Abbas, N., & Shatanawi, W. (2022). Theoretical survey of time-dependent micropolar nanofluid flow over a linear curved stretching surface. *Symmetry*, 14(8), 1629. doi: 10.3390/sym14081629

[9] Majeed, A., Naeem, S., Zeeshan, A., Qayyum, A., & Alhodaly, M.S. (2024). Three-dimensional bio-convection mechanism and heat transportation of nanofluid induced by magnetic field. *International Journal of Modern Physics B*, 38(20), 2450258. doi: 10.1142/S0217979224502588

[10] Abbas, Z., Arslan, M.S., & Rafiq, M.Y. (2024). Numerical investigation of cilia beating modulated flow of magnetized viscous fluid

in a curved channel with variable thermal conductivity. *Alexandria Engineering Journal*, 97, 230–240. doi: 10.1016/j.aej.2024.04.018

[11] Mahesha, R., Nalinakshi, N., & Kumar, T.S. (2025). Numerical study of radiative MHD hybrid nanofluid flow through porous concentric cylinders. *Archives of Thermodynamics*, 46(1), 201–208. doi: 10.24425/ather.2025.154194

[12] Ahmad, S., Nadeem, S., & Muhammad, N. (2019). Boundary layer flow over a curved surface imbedded in porous medium. *Communications in Theoretical Physics*, 71(3), 344–348. doi: 10.1088/0253-6102/71/3/344

[13] Riaz, A., Khan, S.U.D., Zeeshan, A., Khan, S.U., Hassan, M., & Muhammad, T. (2021). Thermal analysis of peristaltic flow of nanosized particles within a curved channel with second-order partial slip and porous medium. *Journal of Thermal Analysis and Calorimetry*, 143, 1997–2009. doi: 10.1007/s10973-020-09454-9

[14] Adeyemo, A.S., Sibanda, P., & Goqo, S.P. (2024). Analysis of heat and mass transfer of a non-linear convective heat generating fluid flow in a porous medium with variable viscosity. *Scientific African*, 24, e02140. doi: 10.1016/ j.sciaf.2024.e02140

[15] Sonam & Yadav, R.S. (2024). Evaluating the mixed convection flow of Casson fluid from the semi-infinite vertical plate with radiation absorption effect. *Archives of Thermodynamics*, 45(4), 45–59. doi: 10.24425/ather.2024.151996

[16] Jagadha, S., Madhusudhan Rao, B., Durgaprasad, P., Gopal, D., Prakash, P., Kishan, N., & Muthunagai, K. (2024). Darcy-Forchheimer two-dimensional thin flow of Jeffrey nanofluid with heat generation/absorption and thermal radiation over a stretchable flat sheet. *Archives of Thermodynamics*, 45(2), 247–259. doi: 10.24425/ather.2024.150869

[17] Imtiaz, M., Nazar, H., Hayat, T., & Alsaedi, A. (2020). Soret and Dufour effects in the flow of viscous fluid by a curved stretching surface. *Pramana − Journal of Physics*, 94, 48. doi: 10.1007/s12043-020-1922-0

[18] Konwar, H., Bendangwapang, & Jamir, T. (2022). Mixed convection MHD boundary layer flow, heat, and mass transfer past an exponential stretching sheet in porous medium with temperature-dependent fluid properties. *Numerical Heat Transfer, Part A: Applications*, 83(12), 1346–1364. doi: 10.1080/10407782.2022.2104581

[19] Jamir, T., Konwar, H., & Tzudir, B. (2024). Soret and Dufour effects on unsteady non-linear mixed convection flow past a stretching sheet influenced by non-linear thermal radiation. *Numerical Heat Transfer, Part A: Applications*, 86(14), 4987–5005. doi: 10.1080/10407782.2024.2325675

[20] Krishnaveni, T.R., Reddy G.V.R., Anitha, J., Kumar G.C., Rajagopalan, N.R., Govindan, V., Byeon, H., Pimpunchat, B. (2025). Mechanism of thermal radiation, Soret-Dufour on ferromagnetic hybrid nanofluid through a permeable surface. *Case Studies in Thermal Engineering*, 68, 105919. doi: 10.1016/j.csite.2025.105919

[21] Haile, E., & Shankar, B. (2014). Heat and mass transfer through a porous media of MHD flow of nanofluids with thermal radiation, viscous dissipation and chemical reaction effects. *Chemical Science International Journal*, 4(6), 828–846. doi: 10.9734/acsj/2014/11082

[22] Oladapo, A.O., Akindele, A.O., Obalalu, A.M., & Ajala, O.A. (2024). Important of slip effects in non-Newtonian nanofluid flow with heat generation for enhanced heat transfer devices. *Defect and Diffusion Forum*, 431, 147–162. doi: 10.4028/p-baACr1

[23] Sademaki, L.J., Reddy, B.P., & Matao, P.M. (2025). Viscous dissipation effects on heat propagating MHD nanofluid flow induced by the Brownian motion and thermophoresis impacts in a vertical cone with convective surface conditions. *Partial Differential Equations in Applied Mathematics*, 13, 101143. doi: 10.1016/j.padiff.2025.101143

[24] Hanafy, H., & Tlili, I. (2025). Thermo-diffusion analysis for viscoelastic fluid due to stretching surface with viscous dissipation and radiative effects. *Case Studies in Thermal Engineering*, 67, 105848. doi: 10.1016/j.csite.2025.105848

[25] Shampine, L., Kierzenka, J., & Reichelt, M. (2000). Solving boundary value problems for ordinary differential equations in MATLAB with bvp4c. *Tutorial Notes*, 752751–27. https://classes.engineering.wustl.edu/che512/bvp_paper.pdf